Transient electron energy distribution in supported Ag nanoparticles

New Journal of Physics
An Institute of Physics and Deutsche Physikalische Gesellschaft Journal

Transient electron energy distribution in supported Ag nanoparticles

M Merschdorf, C Kennerknecht, K Willig and W Pfeiffer
Physikalisches Institut, Universität Würzburg, D-97074 Würzburg, Germany
E-mail: pfeiffer@physik.uni-wuerzburg.de

New Journal of Physics **4** (2002) 95.1–95.15 (http://www.njp.org/)
Received 13 August 2002
Published 15 November 2002

Abstract. The electron relaxation in Ag nanoparticles supported on graphite is investigated by time-resolved multiphoton photoemission spectroscopy. The photoemission spectra map the transient electron energy distribution in the nanoparticles and reveal the internal thermalization and cooling of the electron gas. The excess energy stored in the electron gas is calculated using the free-electron model. In contrast to the behaviour of isolated nanoparticles the energy loss rate from the electron gas increases with the pump fluence. This indicates that the electron gas equilibration in Ag nanoparticles on graphite is modified by excited electron transport.

1. Introduction

The properties of nanostructured interfaces differ from homogeneous films or bulk material. This makes them interesting for many applications, as e.g. catalysis. Nanoparticles supported on a substrate are used as model catalysts and it was found that the particle size influences their chemical reactivity [1]–[3]. However, the underlying mechanisms for this size-dependent catalytic activity are not yet fully understood. In addition, it is known that a hot electron gas, that is not in equilibrium with the lattice, can induce chemical surface reactions that are inhibited under equilibrium conditions [4]. Accordingly, the relaxation behaviour of excited electrons can strongly influence the reactivity of an interface and it is therefore important to gain insight into how nanostructuring influences electronic relaxation at interfaces. However, the investigation of electron relaxation is up to now limited to homogeneous bulk material or thin films. Here we demonstrate that time-resolved two-photon photoemission spectroscopy provides a probe for the transient non-equilibrium electron energy distribution in supported nanoparticles and, therefore, allows an investigation of the influence of three-dimensional electron confinement and coupling to the substrate on the electron relaxation.

1367-2630/02/000095+15$30.00

Electron–electron, electron–surface and electron–phonon scattering events determine the relaxation of non-equilibrium electrons in metals. Time-resolved reflection or absorption measurements [5, 6] and two-photon photoemission spectroscopy [7]–[10] have been used to investigate the response of the electron gas in metals directly in the time domain. All these techniques are based on the pump–probe scheme, i.e. a first ultrashort laser pulse excites the system and a second time-delayed laser pulse monitors the effect of the first one. The optical excitation with a laser pulse leads to a transient perturbation of the electron distribution. The pure optical methods, e.g. reflection and transmission measurements, indirectly monitor this transient electron distribution via the change of the dielectric function $\varepsilon(\omega)$ [11]. Therefore, their interpretation is based on relating the non-equilibrium electron distribution to $\varepsilon(\omega)$. In contrast, time-resolved two-photon photoemission spectroscopy reveals directly the occupation of intermediate states and therefore provides energy-resolved information on the evolving electron distribution [7, 12].

Most time-resolved experiments are performed either with bulk material [10, 13]–[15], thin films [5, 7, 16]–[18] or isolated nanoparticles [19]–[22]. The geometry has a strong impact on the relaxation behaviour of the excited electrons. For bulk material the finite penetration of the pump excitation, the ballistic transport of excited electrons and, on a longer timescale, the heat transport influence the electron relaxation. In thin films these influences are modified and the cooling rate of the electron gas is slower than in bulk material or in films of a thickness exceeding the mean free path of excited electrons [23]. In small isolated nanoparticles, i.e. either free particles in the gas phase or embedded in a dielectric matrix, the transport of ballistic electrons becomes unimportant, since the excitation is homogeneous over the nanoparticle. The relaxation dynamics in metal nanoparticles embedded in a dielectric has been investigated thoroughly by transient optical absorption (for recent reviews see [24]–[27]). Depending on the wavelength the transient absorption measurement probes different regions in the metal band structure, either monitoring the energy loss from the electron gas by interband transitions or the initial thermalization by using a probe photon energy at the onset of the intraband absorption [28].

In contrast to isolated nanoparticles, the electron relaxation in supported nanoparticles is also influenced by electron transfer processes between substrate and nanoparticle (figure 1). A metal nanoparticle on a conductive substrate or a thin oxide layer couples electronically and the coupling strength determines the transmission probability for electrons. Under equilibrium conditions the transfer in both directions will cancel. However, a net flow of electrons can arise if a non-equilibrium condition is generated by the absorption of a laser pulse. Note that the transmission probability for excited electrons increases strongly with the electron energy, since the effective barrier height for electron tunnelling is reduced. Accordingly, the interface between nanoparticle and substrate can influence the electron energy distribution in the nanoparticles in a complex manner. In particular, the impact of this electron transfer depends strongly on the electron energy. Beside the tunnel probability the charge transfer is also influenced by the capacitance and transient charge of the supported nanoparticle. For sufficiently small electron energies transfer might be impossible due to the Coulomb blockade [29]. Time-resolved two-photon photoemission provides energy-resolved information about the transient electron distribution and is therefore a valuable tool to investigate the electron relaxation and transient energetic shifts in a heterogeneous system.

Time-resolved two-photon photoemission can be extended to the investigation of nanostructured surfaces by tuning the laser excitation to a specific resonance, e.g. the surface plasmon excitation in Ag nanoparticles on graphite [30]–[32]. For resonant excitation the total

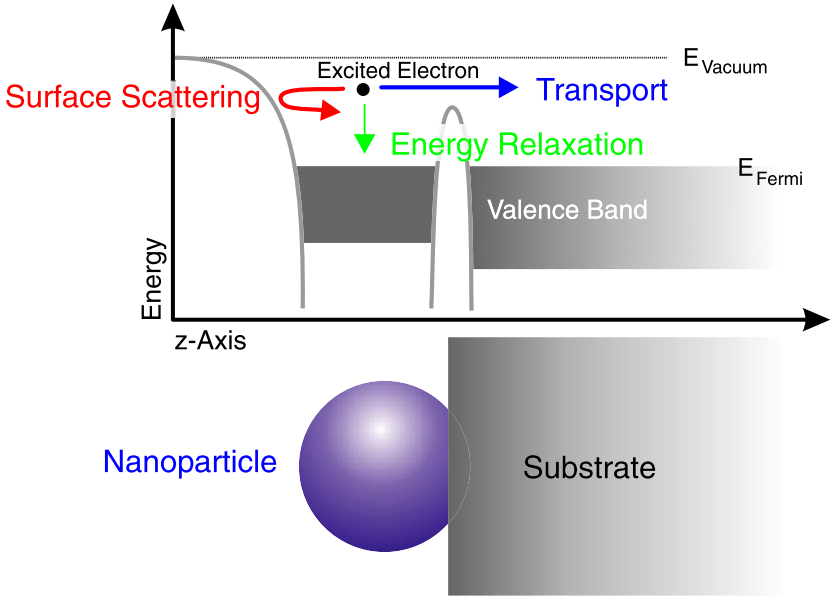

Figure 1. Schematic representation of the mechanisms that control the relaxation of excited electrons in supported nanoparticles.

photoemission yield is dominated by the emission from the nanoparticles and it has been recently demonstrated that the electron gas temperature T_{el} and the cooling of the electron gas can be monitored in time-resolved experiments [33]. The basic pump–probe scheme is depicted in figure 2. The irradiation of the sample with an ultrashort laser pulse at 780 nm is not resonant with the surface plasmon and therefore leads to the formation of a non-equilibrium electron distribution in the graphite substrate and in the Ag nanoparticles. The partitioning of the absorbed pump fluence on nanoparticles and substrate is difficult to assess, since reflectivity measurements provide only an upper limit for the absorption in the nanoparticles of about 0.3% (compare section 2). The transient behaviour of the electron distribution in the nanoparticles after the absorption of the pump pulse is monitored by a two-photon excitation of the nanoparticles at 3.2 eV photon energy (390 nm). This photon energy is close to the surface plasmon resonance of the supported nanoparticles at about 3.4 eV [32] and it has been recently demonstrated that under these conditions the photoemission yield is dominated by the emission from the nanoparticles [31].

The pump pulses at 1.6 eV photon energy (780 nm) excite electrons in a one-photon process from occupied states to unoccupied states above E_F. The initial states are located between the Fermi energy E_F and $E_F - 1.6$ eV. The resulting non-equilibrium electron energy distribution is shown in figure 2 schematically as a stepped electron energy distribution $f_{\mathrm{Ag}}(E)$ for the Ag nanoparticles. As mentioned above, transport and scattering events lead to rapid relaxation of this nonequilibrium state. In about 1 ps the initial distribution evolves into a smooth distribution, that is well described by a Fermi distribution function with an elevated temperature. After this initial thermalization, it is therefore possible to characterize the electronic excitation by a single parameter, i.e. T_{el}. However, the electron gas is not yet in equilibrium with the lattice and on a longer timescale of several ps the electron gas in the nanoparticles loses energy due to electron–phonon scattering and transport of excited electrons.

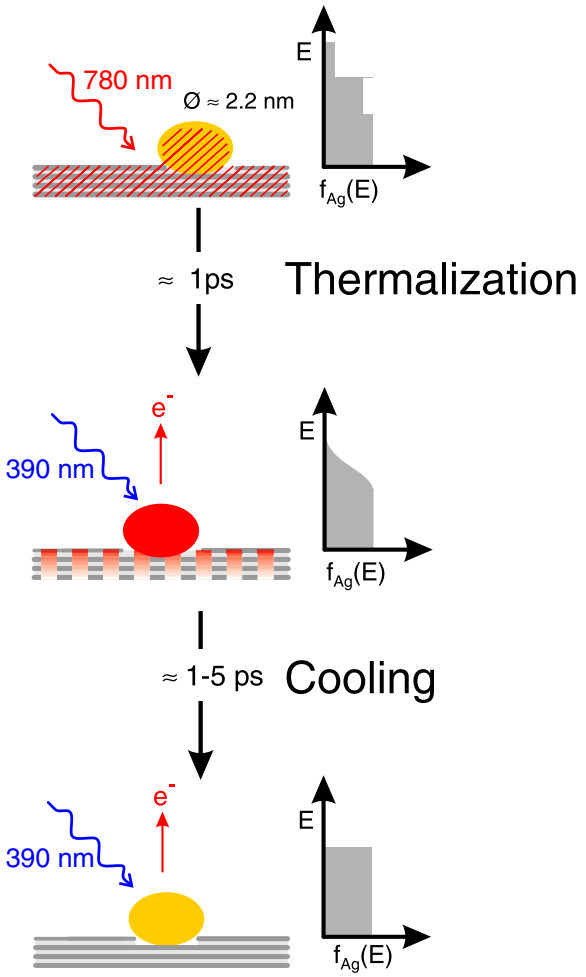

Figure 2. Pump–probe scheme for time-resolved photoemission spectroscopy of the electron relaxation in supported nanoparticles.

2. Experimental method

The nanoparticles were prepared following the procedure given in [34]. Cleaved highly oriented pyrolytic graphite (HOPG) is sputtered with Ar ions (1 keV, 10^{11} cm^{-2}) and oxidized in air ($T = 520\,^{\circ}$C, 20 min) thereby forming pits in the topmost layer of the graphite. Silver is evaporated onto the sample (0.1 Å s^{-1}, 10 s, 350 °C), condenses into the pits and forms particles of several nanometres in size. An *in situ* scanning tunnelling microscope allows the determination of the height distribution of the nanoparticles that exhibits typically a relative width of about 25%. Time-resolved two-photon photoemission spectroscopy is performed using the output of an amplified Ti:sapphire laser system (1.6 eV, 60 fs pulse duration, repetition rate 100 kHz) and its second harmonic (3.2 eV, 50 fs pulse duration) as pump and probe pulses, respectively.

The pump photon energy is far detuned from the surface plasmon resonance of the supported Ag nanoparticles and hence the pump pulse absorption in the substrate and the nanoparticles has to be considered. Reflectivity measurements show that the reduction of reflectivity at the pump photon energy due to the presence of nanoparticles is smaller than our experimental resolution

of about 0.3%. Together with the surface coverage with nanoparticles of about 2% this allows us to estimate an upper limit for the fraction of the fluence absorbed in the nanoparticles. Less than 15% of the incident fluence that hits a nanoparticle is absorbed in the nanoparticle. Accordingly, the dominant part of the pump pulse is absorbed in the graphite substrate. This energy, however, is deposited over the penetration depth of the incident light of about 35 nm. The probe pulses are attenuated so that the shape of the obtained two-photon photoemission spectrum does not depend on laser intensity and heating by the probe pulse is prevented (probe fluence <0.1 mJ cm^{-2}).

For time-resolved studies, pump and probe pulses are delayed with respect to each other. The focus of the pump pulse (30 μm diameter) has been chosen larger than the focus of the probe pulse (20 μm diameter) in order to minimize temperature gradient effects. The samples are mounted on an UHV manipulator with good thermal contact to a large thermal reservoir. The experiments are all performed at 300 K. The average temperature rise of the sample is smaller than the uncertainty of the experimentally determined electron gas temperature of about 50 K. The kinetic energy of the emitted photoelectrons is analysed using a time-of-flight spectrometer. Electrons for all kinetic energies are recorded simultaneously. To minimize the influence of small variations of the laser power in the pump–probe signal the delay is scanned repeatedly. During this averaging over typically 10 h the laser pulse duration and laser power are continuously monitored. The total variation of both is smaller than 5%. Incremental pump–probe scans and photoelectron spectra recorded before and after the scan ensure that the surface properties are not altered during the scan.

3. Experimental results

In time-resolved two-colour pump–probe experiments different excitation pathways contribute to the photoemission yield. Figure 3 displays the photoemission spectrum obtained for negative delay (reference) and for simultaneous pump and probe pulses. The reference spectrum reflects the electron energy distribution undisturbed by the pump pulse, since the probe pulse precedes the pump pulse and the pump pulse alone does not lead to photoelectron emission. As pointed out in the introduction, under probe excitation the photoemission is dominated by the nanoparticles and therefore the shape of the photoemission spectrum reflects the electron energy distribution in the nanoparticles. No single-photon photoemission is observed, since the work function of the surface is 4.4 eV. The shape of the photoemission spectra allows us to identify four different multiphoton excitation processes. For kinetic electron energies up to about 2 eV the reference spectrum is dominated by two-photon photoemission (process (1) in figure 3(b)). The kink in the spectrum at about 2 eV kinetic energy corresponds to the two-photon photoemission from initial states close to E_F. For higher kinetic energy the photoelectron yield decreases further and reaches the noise limit at about 3.5 eV. These electrons originate from a three-photon excitation process (process (2) in figure 3(b)) since the photoemission yield in the energy range between 2 and 4 eV varies with the third power of the laser fluence dependence. The spectrum obtained for simultaneous pump and probe pulses exhibits two distinct differences to the reference spectrum: the photoemission yield for kinetic energies below 0.5 and above 2 eV is increased. The sum of pump and probe photon energy is 0.4 eV larger than the work function and therefore the higher photoemission yield at low kinetic energy is attributed to the absorption of one pump and one probe photon (process (3) in figure 3(b)). Similarly, the increase of the photoemission yield at energies above 2 eV reflects the absorption of one pump and two probe photons (process (4) in figure 3(b)). It is important to note that the absorption of two pump photons (1.6 eV) does not

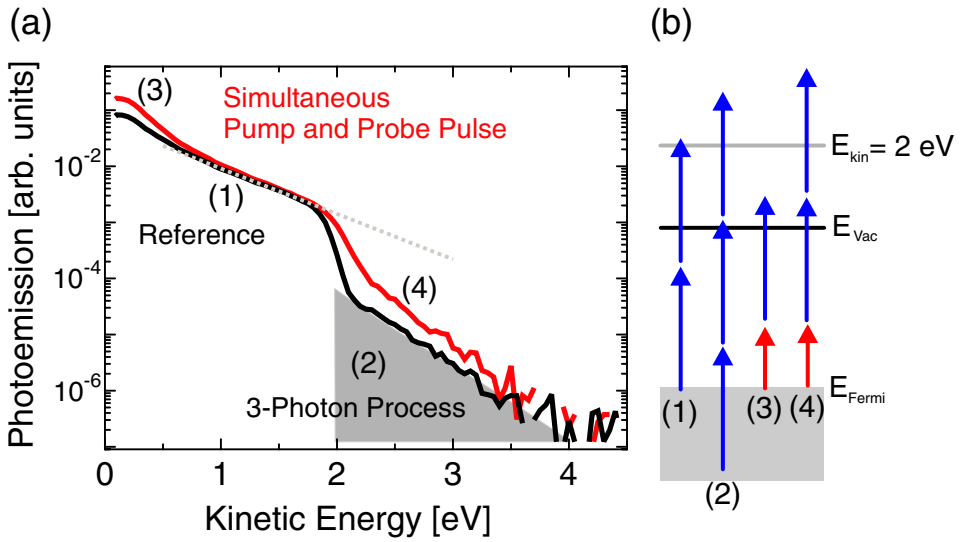

Figure 3. (a) Photoemission spectra for the excitation of Ag nanoparticles on graphite with pump and probe pulses at 780 and 390 nm, respectively. The average height of the nanoparticles is 2.2 nm. Reference spectrum with no influence of pump pulse for negative delay between pump and probe pulse (black curve) and spectrum for zero delay (red curve). The shaded area indicates the photoemission contribution due to three-photon excitation at 390 nm. Four different excitation pathways are schematically represented in part (b) and the corresponding features in the spectra are indicated in part (a). The different excitation mechanisms are further explained in the text.

influence the photoemission spectrum. This process would increase the photoemission yield in the energy range between 1 eV to 1.8 eV, with respect to the reference spectrum. This is not observed in the experiment and we therefore conclude that the pump process is dominated by single-photon absorption.

The spectral shape of the photoemission spectra shown in figure 3 is related to the electron energy distribution $f_{\mathrm{Ag}}(E)$ in the Ag nanoparticles. In the following we present a normalization of the spectra that allows $f_{\mathrm{Ag}}(E)$ to be extracted from the spectra. The three-photon contribution is present in all spectra as a time-independent background. It is therefore determined in the reference spectrum and then subtracted from all spectra of the pump–probe scan. Note that the three-photon contribution is about two orders of magnitude smaller than the two-photon photoemission yield. The shape of the photoemission spectrum after subtracting the three-photon contribution is determined by

(a) the initial electron energy distribution,
(b) the joint density of states for the two-photon excitation probe process,
(c) the lifetime of intermediate and final states,
(d) the photoelectron escape probability and
(e) the spectrometer acceptance and transmission.

The photoemission spectrum for kinetic energy range between 1 and 1.8 eV is independent of the delay between pump and probe pulse. It is well represented by a single exponential (grey dotted curve in figure 3(a)). Assuming that the quantities (b)–(e) vary smoothly with energy, one can extrapolate their behaviour also to initial-state energies above E_F. Normalization of the resulting two-photon photoemission spectrum to the extrapolated exponential (dotted grey curve in figure 3) eliminates the influence of the joined density of states, the variation of the escape probability and spectrometer transmission and yields a quantity that is closely related to the electron energy distribution in the Ag nanoparticles. In the following we show that the described spectrum normalization yields results that are consistent with an independent calibration of the spectral shape [33] and allow a quantitative assessment of the excess energy stored in the electron gas. Therefore, the spectrum normalization which is based on the extrapolation of the spectral shape for states above E_F indeed yields the transient electron energy distribution $f_{\mathrm{Ag}}(E)$.

Normalized photoemission spectra are shown in figure 4 for the reference and for simultaneous pump and probe pulses obtained at two different pump fluences. The normalized reference spectrum is constant for initial states below E_F and then drops rapidly to the noise level with increasing initial-state energy. For zero delay between pump and probe pulse the decrease of the spectrum is less abrupt and a tail of the distribution extends far above E_F. The photoemission yield in this tail increases linearly with incident pump fluence, i.e. about a fourfold increase of the incident pump fluence leads to the same increase of the photoemission yield.

The normalized spectra for initial states close to E_F can be well described by a phenomenological fitting function $f_{\mathrm{Ag}}(E, T_{el}, w)$ that is obtained as a convolution of the Fermi distribution function $f_F(E, T_{el})$ and a normal distribution $g(E, w)$ that accounts for the finite spectral resolution w in the experiment:

$$f_{\mathrm{Ag}}(E, T_{el}, w) = f_F(E, T_{el}) * g(E, w) = \left(\mathrm{e}^{\frac{E-E_F}{k_B T_{el}}} + 1\right)^{-1} * \left(N\mathrm{e}^{-\frac{E^2}{2w^2}}\right), \qquad (1)$$

with the electron gas temperature T_{el}, the Boltzmann constant k_B, and a normalization factor N. Both the spectral resolution w and the electron gas temperature T_{el} determine the width of the Fermi edge in the photoemission spectrum. The spectral resolution w is independent of the pump–probe delay and, therefore, w is determined once for the reference spectrum recorded at 300 K sample temperature for large negative pump–probe delay ($\tau = -5$ ps). For the other spectra of one pump–probe scan w is then held fixed at this value and T_{el} is determined as a function of pump–probe delay by fitting the spectra. The spectral broadening parameter w shows some variation between different experiments but is not influenced systematically by the pump fluence. For spectra at zero pump–probe delay the shape of the spectrum up to $E_F + 0.3$ eV is well described by $f_{\mathrm{Ag}}(E, T_{el}, w)$ (equation (1)), however now for an increased T_{el}. For higher initial-state energy the photoemission yield is substantially higher than is expected for a thermalized electron distribution. This difference between the spectrum and $f_{\mathrm{Ag}}(E, T_{el}, w)$ reflects electrons that have been excited by the pump pulse, but are not yet in equilibrium with the rest of the electrons. According to this, a fit of the spectrum for initial-state energies up to $E_F + 0.3$ eV using equation (1) allows to determine both the elevated electron gas temperature T_{el} and the non-thermal electron distribution (shaded areas in figure 4).

In recent experiments it has been demonstrated by recording the two-photon photoemission spectra for varying sample temperature that T_{el} determined by fitting the photoemission spectra using equation (1) does indeed reflect the actual temperature of the electron gas [33]. The variation of the shape of the spectrum as a function of the sample temperature provides a calibration for the determination of the electron gas temperature [33]. According to this, the

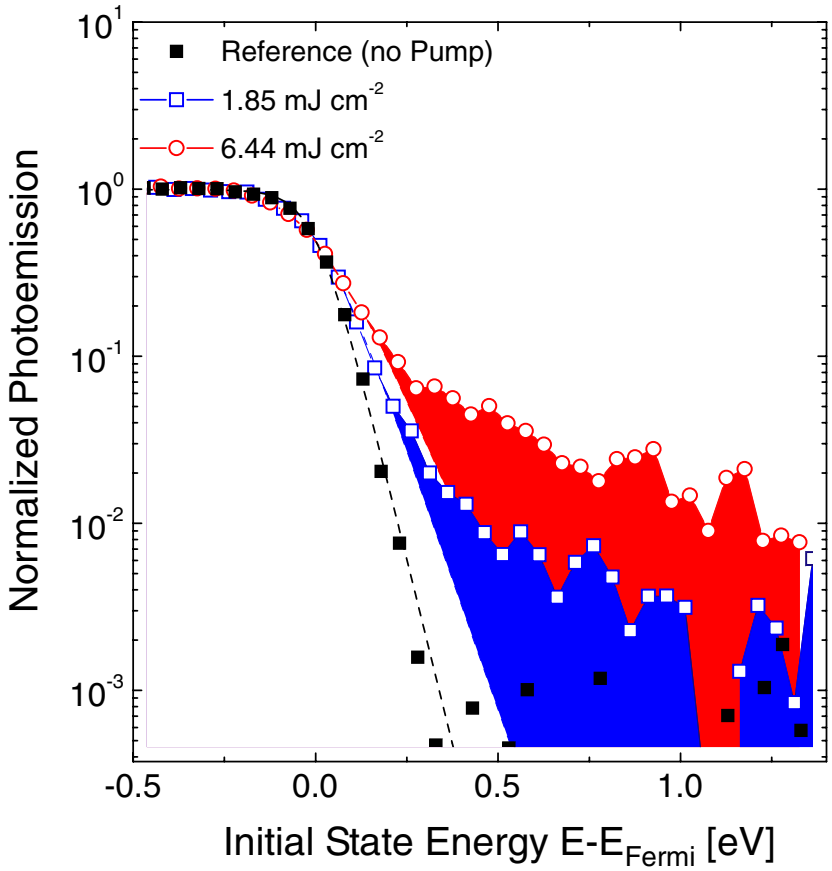

Figure 4. Normalized photoemission spectra for negative delay between pump and probe (reference) and simultaneous pump and probe for two different incident pump fluences. The fit of a spectrally broadened Fermi distribution function to the data is shown as dashed curves. The shaded areas represent the non-thermal electron energy distribution.

normalized photoemission spectrum directly reflects the electron energy distribution for initial states close to E_F. For an initial-state energy higher than about $E_F + 0.3$ eV this is difficult to prove. However, the observation that the three-photon photoemission contribution exhibits no distinct spectral features indicates that the normalization yields a good estimate for the electron distribution over a much broader energy range.

In the following we assume that the normalized photoemission spectrum does indeed reflect the electron energy distribution. The time-resolved pump–probe experiment then provides direct information about the internal thermalization of the electron gas and its cooling. Figure 5(a) shows a contour plot of the transient differential electron energy distribution, i.e. the difference between the transient normalized photoemission spectrum and the normalized reference spectrum. At zero delay the spectra shift to about 0.05 eV higher energy. For the spectra shown in figure 5 this small shift has been corrected in order to yield a contour plot that directly reflects the differential distribution. At negative delay τ the spectral shape is constant. At $\tau = 0$ ps the pump pulse decreases the population in states below E_F and increases the population in states above E_F. The contour line for $\Delta f_{\mathrm{Ag}}(E) = 0.01$ shows the rapid relaxation of the electrons excited far above E_F, reflecting the internal thermalization of the electron gas.

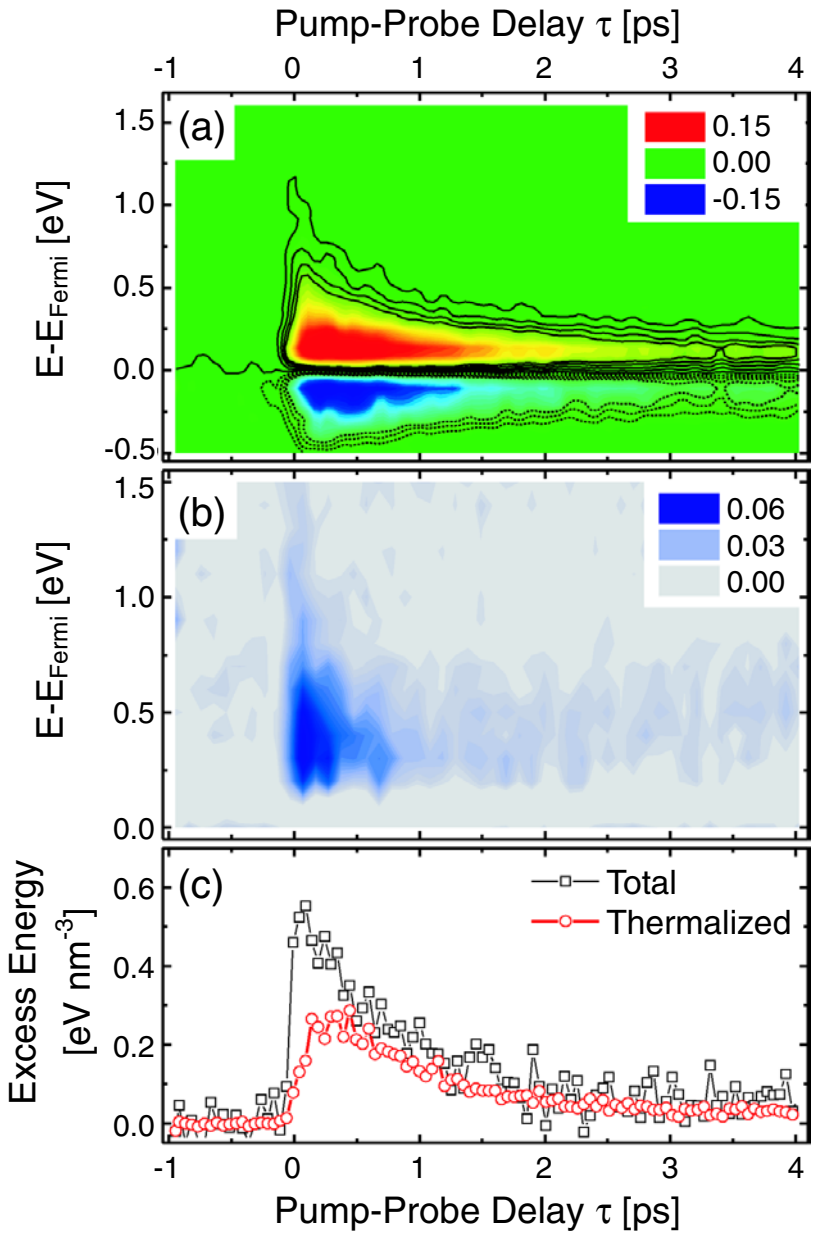

Figure 5. Two-colour pump–probe experiment on Ag nanoparticles (average height 2.2 nm) supported on HOPG using an incident pump fluence of 6.4 mJ cm^{-2} (780 nm centre wavelength, 60 fs pulse duration) and 0.02 mJ cm^{-2} probe fluence (390 nm centre wavelength). (a) Contour plot of the difference between the transient normalized spectra and the reference spectrum recorded at -2 ps delay. The contour lines cover the range from $f(E) = -0.04$ to 0.04 and are spaced by $\Delta f = 0.01$. Contours for negative values are dotted. (b) Transient non-thermal electron distribution represented as a contour plot of the difference between the transient normalized spectra and the thermalized distribution calculated using T_{el} and equation (1). (c) Excess energy density in the electron distribution Δu_{total} and in the thermalized electron distribution $\Delta u_{thermal}$ calculated using equations (2) and (3).

The differential distribution decreases with increasing pump–probe delay and saturates for a delay of about 3 ps at a differential distribution that reflects equilibration of the electron gas with the slightly increased lattice temperature T_l.

As mentioned above, for simultaneous pump and probe pulse, i.e. $\tau = 0$ ps, a non-thermal electron distribution should be visible. However, it is difficult to visualize on a linear scale. Therefore, the transient non-equilibrium distribution is shown in figure 5(b) as a contour plot of the difference between the normalized photoemission spectra and the thermal distribution, i.e. the transient behaviour of the signal represented by the shaded area in figure 4. The transient non-equilibrium distribution extends to about 1 ps. For larger pump–probe delay the non-equilibrium distribution reaches the noise level ($\approx$0.02) and can no longer be distinguished from the thermalized distribution. The non-equilibrium distribution should be also present for energies below E_F. However, for these energies the contribution of this non-equilibrium distribution is smaller than the typical shot noise of the large two-photon photoemission signal. Therefore we show the non-equilibrium distribution only for energies above E_F.

The transient electron distribution contains energy-resolved information about the electron relaxation in the nanoparticles. Based on the free-electron model for a metal, the total excess energy density Δu_{total} of the electron energy distribution is calculated using [35]

$$\Delta u_{total} = \frac{1}{2\pi^2}\left(\frac{2m_{el}}{\hbar^2}\right)^{3/2} \int_0^\infty (E - E_{Fermi})\sqrt{E}\Delta f(E, T_{el})\,\mathrm{d}E, \tag{2}$$

with the free-electron mass m_{el}, and the Fermi energy $E_F = 5.48$ eV [35]. The result is shown in figure 5(c). The total excess energy density rises during the absorption of the pump pulse, and then decreases continuously until it reaches its saturation value. The height distribution of the Ag nanoparticles used for this experiment is centred at 2.2 nm. Assuming spherical particles, the total excess energy corresponds to the absorption of about two pump photons. The total excess energy determined using equation (2) is influenced by the assumption of a free-electron gas. In a real metal the density of states is influenced by the band structure of the metal. However, in the case of silver the quasi-free-electron gas model successfully predicts the optical properties for photon energies up to 4 eV [36]. This and the fact that we observe no distinct spectral features in the multiphoton photoemission spectra from supported nanoparticles supports the assumption of a free-electron gas.

As shown in figure 4, the electron distribution may be separated in a thermalized and a non-thermal distribution. For each spectrum of the pump–probe scan shown in figure 5(a) the thermalized contribution can be characterized by T_{el} as it is determined by fitting the spectra using equation (1). Using the free-electron model the excess energy density of the thermal electron distribution $\Delta u_{thermal}$ is given by [37]

$$\Delta u_{thermal}(T_{el}(t)) = \frac{\gamma_{el} T_{el}(t)^2}{2} - u_{thermal}(T_{el}(t = -\infty) = 300\ \mathrm{K}), \tag{3}$$

with $\gamma_{el} = 3.915 \times 10^{-7}$ eV K^{-2} nm^{-3}. The product $\gamma_{el}\ T_{el}$ is the heat capacity of the electron gas. Within the free-electron model the numerical value of γ_{el} is determined by the density of valence electrons $n_{el} = 58.5$ nm^{-3} and the Fermi energy $E_F = 5.48$ eV [35]. The excess energy density stored in the thermal distribution is also shown in figure 5(c). Compared to the total excess energy density it exhibits a slower rise, reaching its maximum after about 400 fs. Only about half of the absorbed energy density appears in the thermalized electron distribution. The total excess energy density exceeds the energy density in the thermalized distribution up to about 1 ps. After this delay a non-equilibrium electron distribution can no longer be identified and

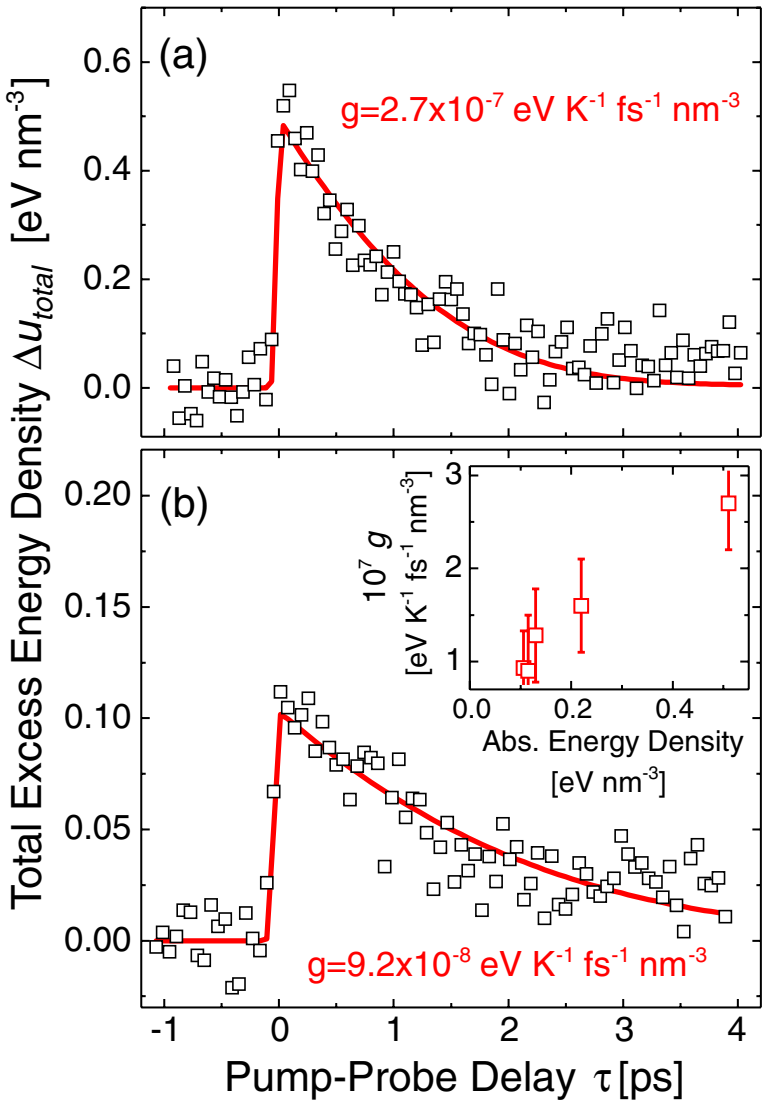

Figure 6. Comparison of transient total excess energy density Δu_{total} in the electron gas (open symbols) and model calculations based on the two-temperature model using optimized parameters for g and the absorbed energy density (red curve). (a) and (b) show the results for incident pump fluence of 6.4 and 1.3 mJ cm^{-2}, respectively. The inset in (b) shows the variation of g with the absorbed energy density.

the excess energy densities determined by the two methods coincide. This is in good agreement with the non-thermal electron distribution shown in figure 5(b) which also extends to about 1 ps.

A decrease of the electron gas cooling rate with increasing electron gas temperature has been observed in time-resolved absorption measurements using isolated metal nanoparticles embedded in a dielectric matrix [27, 38]–[41] and metal films [5, 16, 28]. It is attributed to the increase of the heat capacity of the electron gas with temperature. This mechanism also decreases the excess energy loss rate with increasing total excess energy (see figure 5 in [27]). It is therefore interesting to investigate the fluence dependence of the energy loss rate from supported nanoparticles. In figure 6 the transient excess energy density is compared for different

pump fluences. In contrast to the behaviour of isolated nanoparticles embedded in a dielectric matrix, the experimentally determined energy loss rate increases with the pump fluence. Half of the excess energy is gone after 1 ps for the higher pump fluence, whereas only about one-third is gone for the low pump fluence. In section 4, this unexpected increase of the energy loss rate from supported nanoparticles with increasing absorbed fluence is compared with the prediction of the widely used two-temperature model, providing evidence that the transport of excited electrons via the nanoparticle–substrate interface is crucial for the understanding of electron relaxation in nanoparticles that are electronically coupled to the surrounding, i.e. the substrate.

The results shown up to now demonstrate that two-colour time-resolved two-photon photoemission spectroscopy allows one to distinguish between the non-equilibrium electron distribution and the thermal distribution and directly yields the transient electron energy distribution in supported metal nanoparticles $f_{\mathrm{Ag}}(E,\tau)$. Monitoring the total excess energy density Δu_{total} and the excess energy density stored in the thermalized distribution $\Delta u_{thermal}$ allows both the initial thermalization and the energy loss of the electron gas in the nanoparticles to be followed. The excess energy loss rate increases with absorbed energy. This behaviour is in contrast to the behaviour of isolated nanoparticles, i.e. those that are not in contact with a substrate, and indicates the importance of excited electron transport.

4. Comparison with two-temperature model and discussion

In this section we compare the electron gas cooling in supported nanoparticles with predictions of the two-temperature model for a homogeneously excited bulk material. This model is based on assumptions, e.g. the nonexistence of electron and heat transport, that are not valid for supported nanoparticles. Nevertheless, the comparison allows us to clarify the differences between electron relaxation in supported and isolated nanoparticles embedded in a dielectric matrix.

The two-temperature model is often used to treat the equilibration of an electron gas with the lattice after excitation by a short laser pulse [42]–[44]. Assuming instantaneous thermalization of the initial non-equilibrium electron distribution and based on an energy transfer rate between electron gas and lattice that is proportional to the temperature difference between both reservoirs, one obtains for a homogeneous system two coupled rate equations for $T_{el}(t)$ and the lattice temperature $T_l(t)$

$$\frac{\mathrm{d}T_{el}(t)}{\mathrm{d}t} = -\frac{g}{\gamma_{el}T_{el}}(T_{el}(t) - T_l(t)) + S(t), \tag{4a}$$

$$\frac{\mathrm{d}T_{l}(t)}{\mathrm{d}t} = \frac{g}{c_l}(T_{el}(t) - T_l(t)), \tag{4b}$$

where the source term $S(t)$ reflects the absorption of the pump pulse, g is the electron phonon coupling constant, and c_l is the silver lattice heat capacity (0.0155 eV K^{-1} nm^{-3}). Figure 6 shows the total excess energy density from model calculations using equations (3) and (4) and optimized parameters for g and the absorbed energy density. The fluence dependence of the energy loss rate as discussed in the previous section is also reflected in the optimized values for the electron phonon coupling g, which increase with the absorbed pump fluence (see inset of figure 6(b)). This increase of g cannot be attributed to the initial non-equilibrium electron distribution or to artifacts due to the normalization of the photoemission spectra, since the same behaviour is obtained if the two-temperature model is optimized for $\tau > 1$ ps, i.e. after internal equilibration of the electron gas.

The increase of the energy loss rate from the electron gas or, in terms of the two-temperature model, the increase of the electron phonon coupling g is a surprise. The variation of g is in contrast to the reduction of the cooling time constant with increasing pump fluence that has been observed in metallic nanoparticles embedded in a dielectric matrix [27, 38]–[41] and metal films [5, 28]. This fluence dependence of the cooling rate is attributed to the temperature dependence of the heat capacity of the electron gas and can be explained in the framework of the two-temperature model. However, an increase of g with the pump fluence is in contrast to the behaviour of metal nanoparticles embedded in a dielectric matrix, since for those systems the transient absorption spectra for similar absorbed pump energy densities are well described using a constant g [27]. The electron phonon coupling g for supported nanoparticles should also be independent of the pump fluence, since the absorbed energy density and the size of the nanoparticles in the transient absorption experiments are comparable. Accordingly, the observed fluence dependence of the energy loss rate cannot be explained in the framework of the two-temperature model for an homogeneous system.

Both the two-temperature model for an homogeneous system and the experiments using isolated nanoparticles exclude electron transport phenomena. This might explain the discrepancies between our data on the one hand and two-temperature model predictions and results from isolated particles on the other hand. As mentioned in the introduction, transport of excited electrons might substantially influence the development of the electron distribution in supported nanoparticles. A non-vanishing coupling between nanoparticle and substrate means that electrons are exchanged. As indicated in figure 1, the coupling strength is determined by a tunnel barrier at the interface. The coupling strength and therefore also the transmission probability through the barrier varies with the energy of the electrons, i.e. electrons with high energy couple more strongly and vice versa. According to this, it is expected that the impact of transport on the transient electron energy distribution becomes more important with increasing electron energy. Transport phenomena have been addressed in time-resolved experiments [10, 17, 18, 23, 45] and theoretically [46]. However, a scenario as described above is not covered by these considerations. Knowledge of the transient electron distribution as provided by time-resolved photoemission spectroscopy is crucial for the investigation of the electron transfer between substrate and nanoparticle. In addition, an improved theoretical model for electron relaxation in a nanostructured system, that includes energy dependent transfer rates, is required to gain further insight.

At a closer look, a further discrepancy between the two-temperature model and the experiment is obvious (compare figure 6). For large pump–probe delay the two-temperature model underestimates the excess energy density. Either an about ten times smaller lattice heat capacity compared to bulk Ag or the existence of another source for the heating of the lattice of the nanoparticle besides the electron gas fixes this discrepancy. A significant reduction of the lattice heat capacity in comparison to the bulk value is in contrast to heat capacity measurements for isolated particles [47] and, therefore, rather unlikely for supported nanoparticles. However, in a heterogeneous system like supported nanoparticles the substrate might act as an additional heat source for the nanoparticle, since the pump pulse excites both substrate and nanoparticle. Accordingly, not only does the transfer of electrons influence the electron relaxation in supported nanoparticles, but the phonon coupling between nanoparticle and substrate might also be important. The comparison between the predictions of the two-temperature model and our experiments shows that both the excited electron exchange between substrate and nanoparticle and the transient temperature of the substrate influence the electron gas cooling in supported nanoparticles after non-resonant pulsed laser excitation.

5. Summary

The results shown here demonstrate that two-colour time-resolved two-photon photoemission spectroscopy allows us to investigate the electron relaxation in Ag nanoparticles supported on graphite. The photoemission spectra map the transient electron energy distribution in the nanoparticles, providing information about the internal thermalization of the electron gas and its cooling. It is possible to distinguish between the non-equilibrium electron distribution and the thermal distribution. Based on the free-electron model, the electron distribution yields the excess energy stored in the electron gas. Monitoring the total excess energy and the excess energy stored in the thermalized distribution allows us to follow the initial thermalization and the cooling of the electron gas in the nanoparticles. The excess energy loss rate increases with absorbed energy. This behaviour is in contrast to the behaviour of isolated nanoparticles, i.e. particles that are not in electric contact to the surrounding medium, and cannot be explained in the framework of the two-temperature model for an homogeneous system. This indicates that the electron gas equilibration in Ag nanoparticles on graphite is substantially modified by excited electron transport. In addition, the pump pulse deposits energy in the substrate which then can act as a source for excited electrons and heat. Thus, a model is developed that yields the full transient electron energy distribution and accounts for the absorption of the pump pulse in the substrate and the electron transfer between substrate and nanoparticle.

References

[1] Valden M, Lai X and Goodman D W 1998 *Science* **281** 1647
[2] Sanchez A, Abbet S, Heiz U, Schneider W D, Hakkinen H, Barnett R N and Landman U 1999 *J. Phys. Chem.* A **103** 9573
[3] Frank M, Andersson S, Libuda J, Stempel S, Sandell A, Brena B, Giertz A, Bruhwiler P A, Baumer M, Martensson N and Freund H J 1999 *Chem. Phys. Lett.* **310** 229
[4] Bonn M, Funk S, Hess C, Denzler D N, Stampfl C, Scheffler M, Wolf M and Ertl G 1999 *Science* **285** 1042
[5] Sun C K, Vallee F, Acioli L, Ippen E P and Fujimoto J G 1993 *Phys. Rev.* B **48** 12365
[6] Groeneveld R H M, Sprik R and Lagendijk A 1995 *Phys. Rev.* B **51** 11433
[7] Fann W S, Storz R, Tom H W K and Bokor J 1992 *Phys. Rev. Lett.* **68** 2834
[8] Aeschlimann M, Pawlik S and Bauer M 1995 *Ber. Bunsenges. Phys. Chem.* **99** 1504
[9] Petek H and Ogawa S 1997 *Prog. Surf. Sci.* **56** 239
[10] Knoesel E, Hotzel A and Wolf M 1998 *Phys. Rev.* B **57** 12812
[11] Sun C K, Vallee F, Acioli L H, Ippen E P and Fujimoto J G 1994 *Phys. Rev.* B **50** 15337
[12] Fann W S, Storz R, Tom H W K and Bokor J 1992 *Phys. Rev.* B **46** 13592
[13] Schmuttenmaer C A, Aeschlimann M, Elsayedali H E, Miller R J D, Mantell D A, Cao J and Gao Y 1994 *Phys. Rev.* B **50** 8957
[14] Knoesel E, Hotzel A, Hertel T, Wolf M and Ertl G 1996 *Surf. Sci.* **368** 76
[15] Ogawa S, Nagano H and Petek H 1997 *Phys. Rev.* B **55** 10869
[16] Elsayed-Ali H E, Norris T B, Pessot M A and Mourou G A 1987 *Phys. Rev. Lett.* **58** 1212
[17] Suarez C, Bron W E and Juhasz T 1995 *Phys. Rev. Lett.* **75** 4536
[18] Bonn M, Denzler D N, Funk S, Wolf M, Wellershoff S S and Hohlfeld J 2000 *Phys. Rev.* B **61** 1101
[19] Ahmadi T S, Logunov S L and El-Sayed M A 1996 *J. Phys. Chem.* **100** 8053
[20] Bigot J Y, Merle J C, Cregut O and Daunois A 1995 *Phys. Rev. Lett.* **75** 4702
[21] Hodak J, Martini I and Hartland G V 1998 *Chem. Phys. Lett.* **284** 135
[22] Del Fatti N, Flytzanis C and Vallee F 1999 *Appl. Phys.* B **68** 433
[23] Hohlfeld J, Wellershoff S-S, Güdde U, Conrad U, Jähnke V and Matthias E 2000 *Chem. Phys.* **251** 237

[24] Bigot J Y, Halte V, Merle J C and Daunois A 2000 *Chem. Phys.* **251** 181
[25] Hodak J H, Henglein A and Hartland G V 2000 *J. Phys. Chem.* B **104** 9954
[26] Link S and El Sayed M A 2000 *Int. Rev. Phys. Chem.* **19** 409
[27] Voisin C, Del Fatti N, Christofilos D and Vallee F 2001 *J. Phys. Chem.* B **105** 2264
[28] Del Fatti N, Voisin C, Achermann M, Tzortzakis S, Christofilos D and Vallee F 2000 *Phys. Rev.* B **61** 16956
[29] Barner J B and Ruggiero S T 1987 *Phys. Rev. Lett.* **59** 807
[30] Lehmann J, Merschdorf M, Pfeiffer W, Thon A, Voll S and Gerber G 2000 *J. Chem. Phys.* **112** 5428
[31] Lehmann J, Merschdorf M, Pfeiffer W, Thon A, Voll S and Gerber G 2000 *Phys. Rev. Lett.* **85** 2921
[32] Merschdorf M, Pfeiffer W, Thon A, Voll S and Gerber G 2000 *Appl. Phys.* A **71** 547
[33] Merschdorf M, Pfeiffer W, Voll S and Gerber G 2002 *Phys. Rev. Lett.* submitted
[34] Hövel H, Becker T, Bettac A, Reihl B, Tschudy M and Williams E J 1997 *J. Appl. Phys.* **81** 154
[35] Kittel C 1976 *Introduction to Solid State Physics* 5th edn (New York: Wiley)
[36] Johnson P B and Christy R W 1972 *Phys. Rev.* B **6** 4370
[37] Lugovskoy A V and Bray I 1999 *Phys. Rev.* B **60** 3279
[38] Hodak J H, Martini I and Hartland G V 1998 *J. Phys. Chem.* B **102** 6958
[39] Hodak J H, Henglein A and Hartland G V 1999 *J. Phys. Chem.* **111** 8613
[40] Link S and El-Sayed M A 1999 *J. Phys. Chem.* B **103** 8410
[41] Hodak J H, Henglein A and Hartland G V 2000 *J. Chem. Phys.* **112** 5942
[42] Kaganov M I, Lifshitz I M and Tanatarov L V 1957 *JETP Lett.* **4** 173
[43] Anisimov S I, Kapeliovich B L and Perelman L T 1974 *JETP Lett.* **39** 375
[44] Eesley G L 1986 *Phys. Rev.* B **33** 2144
[45] Aeschlimann M, Bauer M, Pawlik S, Knorren R, Bouzerar G and Bennemann K H 2000 *Appl. Phys.* A **71** 485
[46] Knorren R, Bouzerar G and Bennemann K H 2001 *Phys. Rev.* B **63** 125122
[47] Halperin W P 1986 *Rev. Mod. Phys.* **58** 533